A Comparison of Observed and Model-Derived Structures of Caribbean Easterly Waves

LLOYD J. SHAPIRO

Hurricane Research Division/AOML, NOAA, Miami, Florida

DUANE E. STEVENS AND PAUL E. CIESIELSKI

Department of Atmospheric Science, Colorado State University, Fort Collins, Colorado

(Manuscript received 16 September 1987, in final form 2 November 1987)

ABSTRACT

A linear primitive equation model has been used to test the hypothesis that the vertical structure of observed Caribbean easterly waves is determined by the interaction between convective heating and the environmental wind. The model determines the response to a propagating heat source in a specified basic state. The model allows for the inclusion of diffusion and cumulus momentum transports. The linear perturbations are assumed to have the form of a single Fourier component in the zonal direction. The frequency and zonal wavelength of the disturbance are taken from observations of the three-dimensional structure of a series of Caribbean easterly waves made by Shapiro. The structure of the basic state zonal wind, assumed to be a function of height, is based on observations near the latitude of largest observed wave amplitude. The maximum heating rate is 5 K day^{-1}, centered at about 19°N.

Very good agreement is found between the model-derived vertical structure of the waves and that observed by Shapiro (1986). In particular, the observed 90° westward phase shift between the 200 mb and near-surface troughs, and the westward tilt of the trough axis with height, are reproduced in the model solutions. Although linearization is not strictly valid for the observed wind amplitudes of ~5 m s^{-1}, the model's linear dynamical framework appears to represent the wave's structure well. The westward phase shift is found to depend on the downward flux of wave energy toward a near-critical layer near the ground. Experiments also suggest that the latitude of the disturbance may be as important a factor in the determination of the westward tilt of the trough axis as is the structure of the basic state zonal wind. An eastward tilt of the trough axis in the lower troposphere, such as that in the classical model of a Caribbean easterly wave, can occur at low latitudes, when the westward phase shift is in a narrow layer near the level of maximum heating. Cumulus momentum transports do not substantially change the structure of the forced wave disturbance. The model solutions are compared with similar experiments of Holton, and are related to results of Stevens, Lindzen and Shapiro.

1. Introduction

Once every 3 or 4 days during the summer months, a disturbance propagates westward from Africa across the tropical Atlantic. Most of the systems, which are generally associated with substantial convective activity, continue into the Caribbean. Some may develop circulations that evolve into depressions, then stronger tropical storms and finally hurricanes. Riehl (1954) summarized the properties of easterly waves in the Caribbean, based on several case studies. His description became the "classical" model for these waves. The properties described by Riehl included an eastward tilt of the wave trough axis[1] with height, and a surface trough to the west of the region of maximum precipitation.

Since Riehl's studies, a more complex picture has emerged. Recently, Shapiro analyzed the three-dimensional structure of a series of easterly waves in the Atlantic and Caribbean regions. His study was confined to an analysis of the wind field. In contrast to the classical model presented by Riehl (1954), Shapiro found a westward tilt of the trough axis with height. In particular, both the vorticity and the meridional velocity consistently evidenced a near 90° westward phase shift at 200 mb relative to the lower troposphere. Shapiro (1986) reviewed previous studies that had found a similar westward shift for stronger systems [Colón and Nightingale (1963), Fett (1966), Yanai (1968)]. Burpee (1980), using a composite analysis in the Caribbean region during the GARP Atlantic Tropical Experiment, found a moderate eastward tilt of the trough axis up to ~700 mb, with a strong westward tilt above. As in Shapiro's study, Burpee's composite trough had a 90° westward phase shift of the 200 mb level relative to 700 mb.

Holton (1971) developed a simple model to analyze the structure of linear forced wave disturbances in the

[1] On time-height sections, the easterly wave trough is usually tracked by a shift in the sign of the meridional wind, which is more easily followed than the pressure minimum. The wind or pressure troughs are generally coincident with a maximum in disturbance vorticity, which is also used to define the wave trough.

Corresponding author address: Dr. Lloyd Shapiro, NOAA/ERL, Hurricane Research Division/AOML, 4301 Rickenbacker Causeway, Miami, FL 33149.

presence of vertical shear of the mean zonal wind. The model was used to compare the structures of the waves in different environments. Holton's case I had a resting basic state, while his case II had a mean wind with westerly shear from the surface up to ~12 km. The latter profile was considered to be typical of the easterly trade wind regime. Solutions for case II indicated a surface trough to the west of the heating maximum and an eastward tilt with height. Both features were similar to those described by Riehl (1954). Holton concluded that westerly shear of the mean zonal wind is necessary to produce the classical easterly wave structure. With an easterly shear (his case III), the trough axis tilted westward with height.

The present study provides a comparison of observed and model-derived structures of Caribbean easterly waves. As in Holton's model, the diabatic heat source that drives the waves is specified. Since the convective source is not parameterized in terms of the large-scale fields, feedback from the wave to the heating is explicitly excluded. Thus, the study provides the consistent dynamic structure of the forced wave response, given the convective source, but cannot itself provide a theory for the presence of the coupled wave/convection system. The linear model used to diagnose the waves' structure is described in section 2. This model is more flexible than Holton's, since both boundary layer diffusion and cumulus momentum transports can be included. In section 3, the response to a propagating heat source is evaluated for waves with constant Doppler-shifted frequency. These experiments set the framework for interpretation of the wave structure in a more realistic basic state. The wave parameters and the structure of the mean zonal wind observed in Shapiro's (1986) study are used in section 4. The hypothesis is tested that the vertical structure of the waves observed by Shapiro, including their westward tilt, was determined by the interaction, in the linear dynamical framework, of convective heating and the environmental wind. The role of the vertical flux of energy and the latitude of the heating in determining the structure are evaluated. Section 5 uses a mean zonal wind corresponding to that used in Holton's (1971) case II to isolate the reason for the eastward tilt found in his study and, by inference, in the classical easterly wave model. The results are summarized and discussed in section 6.

2. The model

The model used in the present study was developed by Stevens and Ciesielski (1984). A description of the model is given by Rosenlof et al. (1986). The equations are formulated on a sphere, using the hydrostatic approximation. Primitive equations are used, linearized with respect to a steady basic state. The basic state quantities are designated by an overbar, and the perturbation quantities by a prime. In the present study the basic state wind is purely zonal, $\bar{\mathbf{u}} = (\bar{u}(\theta, z), 0)$, a function of latitude and height. The symbols used here and elsewhere in the paper are listed in appendix A. The basic state wind is assumed to be in gradient thermal wind balance with the temperature field, $\bar{T}(\theta, z)$, which is developed from the Jordan (1958) mean tropical sounding for the hurricane season, applied at the latitude of maximum heating. The linear perturbations are assumed to have the form of a single Fourier component in the zonal direction, proportional to $\exp[i(-\sigma t + s\lambda)]$, with $s > 0$. The model requires specification of the zonal wavenumber and frequency of the forced wave disturbance. For a westward propagating disturbance, $\sigma < 0$.

Vertical diffusion of heat and momentum is incorporated in the model. In addition, cumulus momentum transports can be invoked, as described in detail in appendix C. Neither of these processes were included in Holton's (1971) model. In the present model formulation, some diffusion is required to obtain the numerical solution. A very small "background" kinematic eddy viscosity, $\nu = 1\ \mathrm{m^2\ s^{-1}}$, is used. Even for a vertical scale as small as 1 km, this viscosity is associated with a diffusive time scale > 10 days. In some experiments, enhanced boundary layer diffusion (described below) is also included to represent vertical mixing near the surface.

In all experiments in the present paper the specified diabatic heat source Q' that forces the response has the structure in the meridional plane shown in Fig. 1. The analytic form of the vertical dependence of the heating is given in Eq. (8) of Rosenlof et al. (1986). The heating goes to zero at $p = 150$ and 1000 mb, with a maximum local heating rate of 5 K $\mathrm{day^{-1}}$ located at 400 mb. The vertical level of this maximum is near that typically observed for tropical systems (e.g., see Johnson, 1984). The total vertically integrated heating is chosen to correspond to a maximum perturbation precipitation rate of 1 cm/day. This rate is somewhat less than that used in Holton (1971). The meridional structure of the heating is Gaussian, with a decay scale of 3° lat (about 300 km). The latitude of the maximum heating in Fig. 1 is 9.4°N, though for some experiments the heating will be placed at a higher latitude. The model grid points are indicated on the top and left-hand borders. The model is run with equally spaced grid points in the vertical coordinate, log-pressure (z), with ten grid points per scale height, and in the meridional coordinate, $\sin\theta$, with spacing at the equator about 2° of lat (~200 km).

At the lower boundary, the physical vertical velocity is set to zero, and a bulk aerodynamic parameterization of the surface stress is used, with $(\nu/H)\partial\mathbf{u}'/\partial z = (1.6 \times 10^{-3})(8\ \mathrm{m\ s^{-1}})\mathbf{u}'$; an analogous relation applies to T'. Boundary layer diffusion of momentum and temperature are simulated by inclusion of a surface kinematic coefficient of viscosity and thermal diffusion, $\nu = 25\ \mathrm{m^2\ s^{-1}}$. At $z = 0.1$, the lowest model level above the surface, the value of the coefficient is reduced to one-half of its surface value. Together with the surface stress

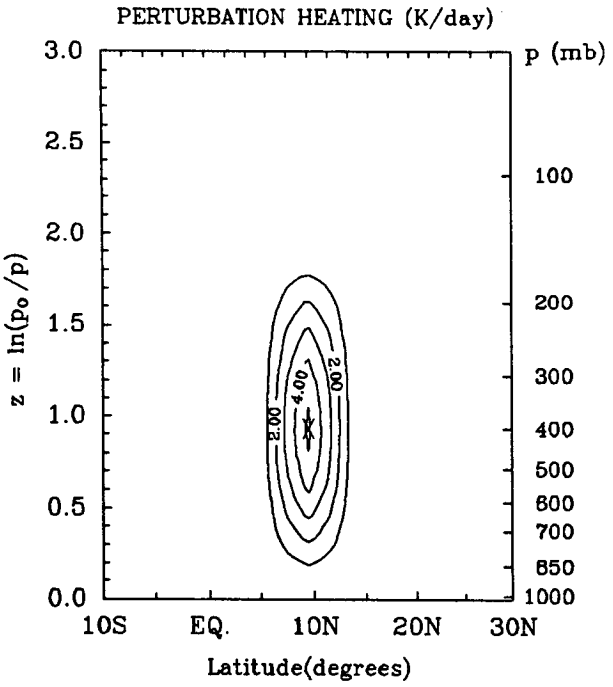

FIG. 1. Distribution of perturbation diabatic heat source, Q'.

parameterization, this value gives an effective damping time for boundary layer friction, and thermal damping, of ~2.1 days.

At the upper boundary, the vertical derivatives of $\mathbf{u}'$, T' and pw' are set equal to zero. In all experiments, except as noted in section 3, the response to the heating decays with height to a small magnitude well below the upper boundary. The meridional velocity is set to zero at the northern and southern boundaries, each about 20° of latitude from the heating maximum. When significant energy appeared near the southern boundary, the domain was extended 20° to the south, and the number of grid points was increased so as to retain nearly the same grid resolution as in the smaller domain. All meridional cross sections will display the entire domain; the location of the maximum heating is marked by an "X". Further details of the model formulation can be found in the report by Stevens and Ciesielski (1984) or the paper by Rosenlof et al. (1986).

3. Constant intrinsic frequency

As a prelude to the use of more realistic basic state zonal wind profiles, the response to the propagating heat source is evaluated in zonal winds that give a constant intrinsic (Doppler-shifted) frequency for the wave. These idealized experiments elucidate the role of the wave period in the determination of the structure of the response, and provide a framework for the interpretation of the more realistic cases. The response to the heating is first evaluated in a resting basic state ($\bar{u} = 0$), as in Holton's (1971) case I. The frequency and wavenumber of the forced wave disturbance are the same as Holton's (1971) values. The parameters for the experiments presented in this paper are summarized in Table 1. The wave period in this first experiment, designated experiment A, is specified to be 5 days. The heating distribution, shown in Fig. 1, is centered at 9.4°N, the closest grid point to the latitude 9°N used in Holton's (1971) experiments. The heating maximum at 400 mb is lower than Holton's maximum at 12 km (about 250 mb), and is more representative of current observational evidence. Neither enhanced boundary layer diffusion nor cumulus momentum transports were included. Although Holton included an explicit scale-independent dissipation (Rayleigh friction and Newtonian cooling) with a damping time of 2.65 days, the present experiment has no such damping. The first two panels in Fig. 2 show the vertical and meridional distribution of the amplitude of the perturbation wind components for experiment A. The following panels show the amplitude and phase at the latitude of maximum heating of the zonal and meridional winds, the vorticity, divergence, geopotential and thermodynamic terms. The phase, which has periodicity of 360°, is displayed so that the heating maximum occurs at phase 0° and east is to the right.

Even though there is no explicit scale-independent dissipation, the results of experiment A are very similar to those of Holton's case I, including the magnitude and distribution of the meridional wind, v'. The max-

TABLE 1. Summary of experiment parameters. Note that all experiments in this Table have no cumulus friction.

Experiment	Figure No.	s	Wave period (days)	Heating lat	Boundary layer viscous ?	$\bar{u}(z)$; intrinsic frequency
A	2	10	5.0	9.4°N	No	$\bar{u} = 0$; $\hat{\sigma} = \sigma = -2\pi/(5$ days)
B	3	11		18.8°N	No	$\hat{\sigma} = -2\pi/(21$ days)
C	5, 6a	11	4.5	18.8°N	25 m^2 s^{-1}	$\bar{u} = \bar{u}_0(z)\cos\theta/\cos(18.8°)$ $\bar{u}_0(z)$ from Fig. 4b (Caribbean)
D	8, 9a	10	5.0	9.4°N	25 m^2 s^{-1}	$\bar{u} = \bar{u}_0(z)\cos\theta$ $\bar{u}_0(z)$ from Fig. 7 (Holton, case II)

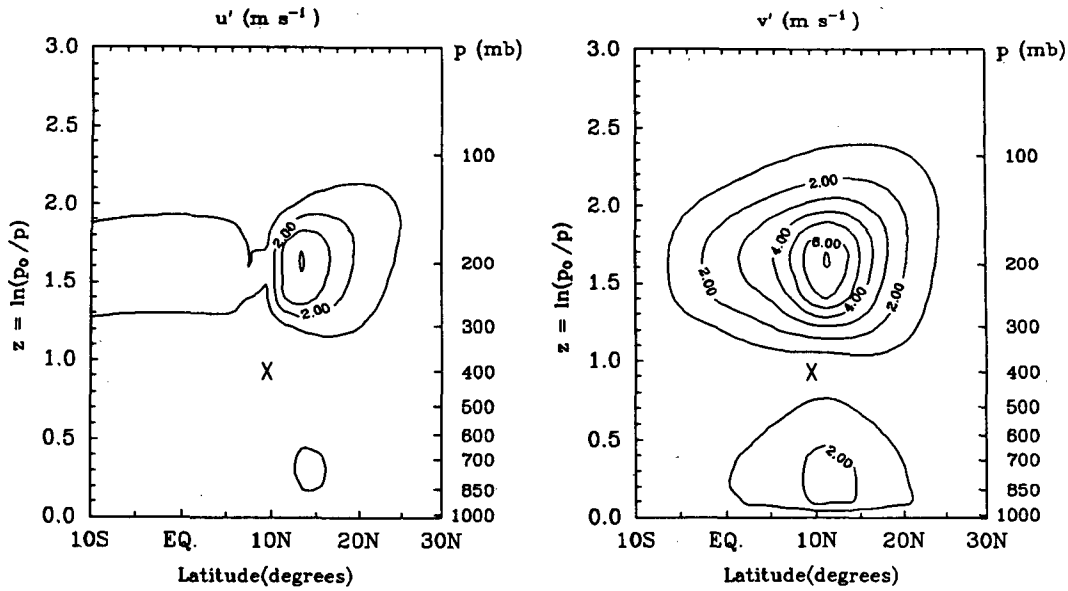

FIG. 2. (a) Experiment A. Meridional and vertical distribution of the amplitude of the zonal wind (u'), and meridional wind (v'). Position of maximum heating is shown by a cross. (b) Experiment A. Amplitude and phase at latitude of maximum heating (9.4°N) of u', v'; vorticity (ζ'); divergence (δ'); geopotential (Φ'); perturbation diabatic heating (Q'); adiabatic cooling ($\bar{\Gamma}w'$); and warming rate ($-i\hat{\sigma}T'$).

imum amplitude of v' in Fig. 2, slightly north of the maximum heating, is 7.0 m s^{-1}. This amplitude is about 1 m s^{-1} less than Holton's maximum, which occurs at the same position. Temperature changes in experiment A are very small, with a maximum warming rate of less than 1 K day^{-1}. Thus, as in Holton's solution, the profile of the vertical velocity, w', follows that of the heating; adiabatic cooling tends to balance the imposed convective heating. Both experiment A and Holton's case I show v' in phase (or 180° out of phase) with the heating, Q'. An inspection of the horizontal structure of the response in experiment A indicates that there is virtually no phase variation with latitude throughout the entire domain. A similar phase structure is evident in Holton's (1971) results for case I (his Fig. 5).

To help us understand the characteristics of the forced wave results, it is useful to consider the horizontal structure equation for an equatorial β-plane:

$$(d^2v'/d\theta^2)/a^2 + L(\theta)v' = 0, \qquad (1a)$$

where

$$L(\theta) = -(2\Omega/a)k/\sigma - k^2 + \sigma^2/(gh) - (2\Omega\theta)^2/(gh)$$
$$[1] \qquad [2] \qquad [3] \qquad [4] \qquad (1b)$$

and h is the equivalent depth [see Eq. (25) of Lindzen, 1967]. The solutions to (1) with positive equivalent depth decay poleward of a turning latitude where the function $L(\theta)$ is zero. The balance of terms in (1b) determines the wave types that are present in the solution. For example, Rossby waves are present when term 3 can be neglected in comparison to terms 1 and 2. On the other hand, gravity waves occur in the high frequency limit so that term 1 is negligible compared to term 3. Furthermore, the complete set of eigenvalues $\{h_n\}$ for (1) includes both positive and negative values. According to Lindzen (1967) the modes with positive equivalent depth correspond to vertically propagating waves that are confined to equatorial regions between two turning latitudes. Negative equivalent depths are characterized by vertically trapped modes whose largest amplitudes are bounded away from the equator; these modes cannot be represented on an equatorial β-plane, and a midlatitude β-plane approximation is in general appropriate.

With this background we are now able to interpret the forced wave results. As noted by Stevens et al. (1977; hereafter referred to as SLS), for the choice of parameters in experiment A, terms 1 and 2 in (1b) exactly cancel so that term 3 cannot be neglected. This particular balance implies that experiment A is treating inertia-gravity waves with turning latitudes at $\sigma = \pm f$ (in this case 6°N and 6°S). The heating specified in experiment A is confined predominately poleward of the turning latitude at 6°N. Thus negative equivalent depths are primarily excited, resulting in vertically trapped modes. Moreover, the narrow heat source used in this case projects primarily onto modes with small equivalent depth [i.e., with $L(\theta)$ large]. Under this circumstance the solution to the vertical structure equation for the vertical velocity tends to follow the heating. Details are given in appendix B. As a result of the small negative equivalent depths, the adiabatic cooling tends to balance the heating and the warming rate is small. Also, the modes are confined to levels near the heating

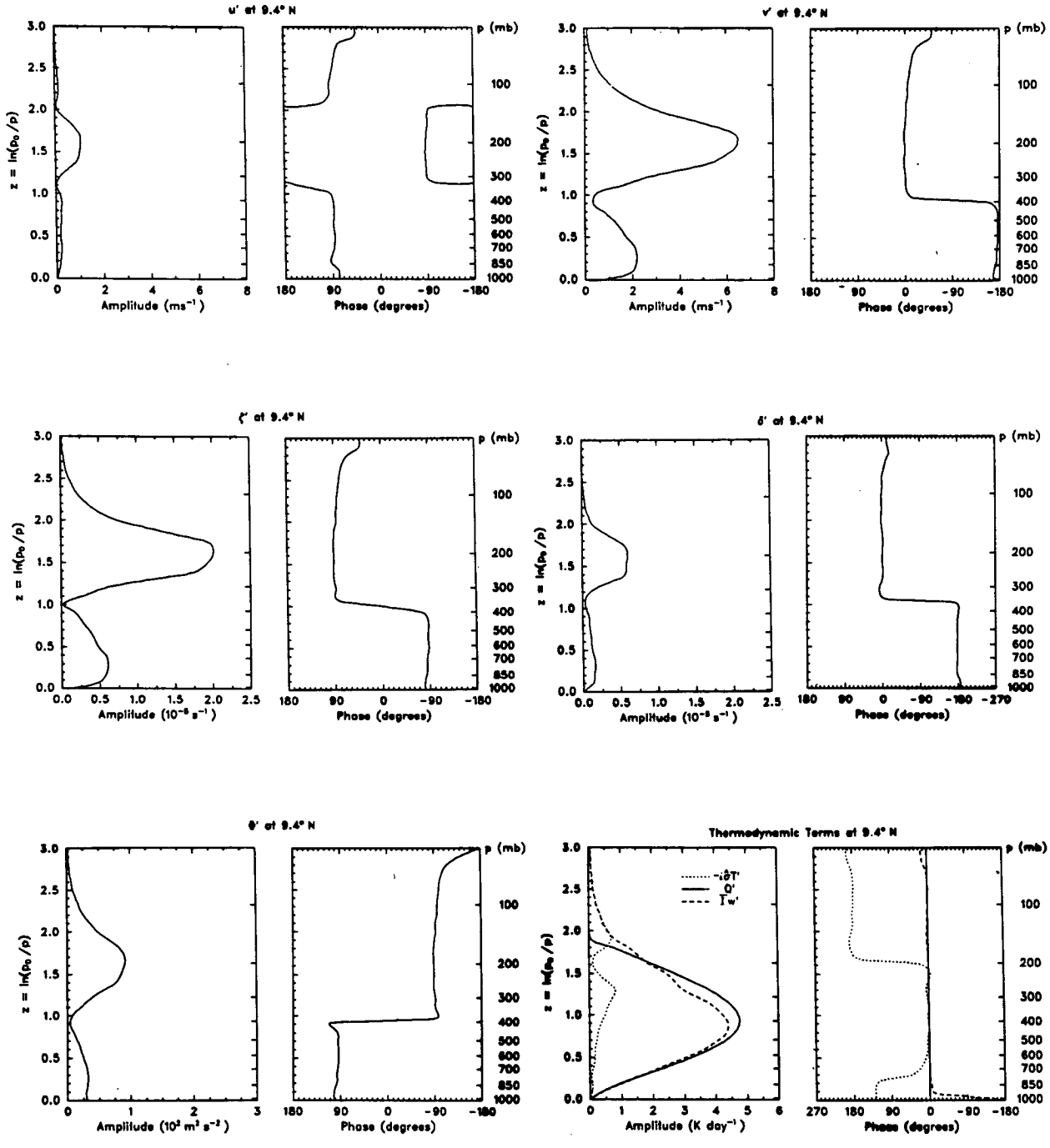

FIG. 2. (*Continued*)

and, in the absence of dissipation, have no phase variation with height. Direct inspection then indicates that the coefficients and boundary conditions of the linearized primitive equations are purely real when put in terms of the variables u', Φ' (the zonal wind and geopotential, respectively), iQ', iw' and iv'. Thus, there is no phase variation with latitude, and u' and Φ' are in quadrature (90° out of phase) with Q', w' and v'. Consistent with the trapped nature of the modes, w' is in quadrature with Φ' so that there is no vertical energy flux (i.e., $\overline{\mathrm{Re}(w')\,\mathrm{Re}(\Phi')} = 0$; see appendix A). Moreover, the vorticity, ζ', is in quadrature with Q', v' and the divergence, δ'.

A more complete understanding of the vorticity structure can be obtained. Holton (1971) did not display the vorticity. Figure 2 shows that the phase of

vorticity in the upper troposphere is 90° to the west of the heating, and 90° to the east of the heating in the lower troposphere. These phase relationships are most easily explained in terms of the vorticity budget.

The perturbation vorticity equation can be written,

$$\underset{[1]}{-i\sigma\zeta'} + \underset{[2]}{ik\bar{u}\zeta'} + \underset{[3]}{\beta v'} + \underset{[4]}{f\delta'} - \underset{[5]}{(\partial\bar{u}/\partial z)(\partial w'/\partial\theta)/a} - \underset{[6]}{\mathbf{k}\cdot\nabla\times\mathbf{D}(u')} - \underset{[7]}{\mathbf{k}\cdot\nabla\times\mathbf{F}_c'} = 0. \quad (2a)$$

Very small terms in (2a) due to the vorticity of the mean zonal wind have been omitted. Diffusion is included in the term [6], where

$$D(\mathbf{u}') = (g/p)(\partial/\partial z)[(\nu p/gH^2)(\partial\mathbf{u}'/\partial z)]. \quad (2b)$$

The effects of cumulus friction are represented by term [7], the curl of the cumulus momentum source terms, $\mathbf{F}_c'$, as specified in appendix C. In the absence of dissipative forces, including cumulus friction, the primary vorticity balance is

$$\underset{[1]}{-i\sigma\zeta'} + \underset{[2]}{ik\bar{u}\zeta'} + \underset{[3]}{\beta v'} + \underset{[4]}{f\delta'} - \underset{[5]}{(\partial\bar{u}/\partial z)(\partial w'/\partial\theta)/a} \approx 0. \quad (3)$$

The terms in (3) are the local vorticity tendency [1], advection by the mean wind [2], advection of planetary vorticity [3], vortex stretching [4], and vortex twisting [5]. The first two terms in (3) can be combined into a single term $-i\hat{\sigma}\zeta'$, where $\hat{\sigma}$ is the wave's intrinsic Doppler-shifted frequency.

When $\bar{u} = 0$, as in experiment A, $\hat{\sigma} = \sigma$ so that the approximate vorticity equation becomes

$$\underset{[1]}{-i\sigma\zeta'} + \underset{[3]}{\beta v'} + \underset{[4]}{f\delta'} \approx 0. \quad (4)$$

For the perturbation response in experiment A, the magnitude of the planetary term is less than that of the local tendency, with $|\beta v'/(\sigma\zeta')| \approx 0.5$. A simple scaling shows that this relationship will generally be satisfied for quasi-geostrophic, synoptic-scale waves: for a wave period of 4 days and wavelength of 3000 km, $|\beta v'/(\sigma\zeta')| \leqslant |\beta/(\sigma k)| \sim 0.5$. Since the profile of w' follows that of the heating, there is convergence below the heating maximum (400 mb) and divergence above. The largest divergence occurs near 200 mb. Then, since $\sigma < 0$ (westward propagation), *and* since v' is in quadrature with ζ', (4) shows that the vorticity phase is 90° to the west of the heating in the region of divergence and 90° to the east in the region of convergence; the vertical phase structure of vorticity seen in Fig. 2 directly results.

The phase structure of experiment A is not sensitive to the latitude of the disturbance. Displacement of the heating maximum to 19°N (results not shown) gives the same phase for all variables as in Fig. 2.

The second experiment (designated experiment B) specifies an intrinsic frequency $-\hat{\sigma} = 2\pi/(21 \text{ days})$. The waves are in the long-period regime studied by SLS and many other idealized theoretical analyses of tropical waves. The response to the convective heating, centered at latitude 19°N, is shown in Fig. 3. The response is very different from that in experiment A. Considerable wave energy is distributed away from the heating. For the small intrinsic frequency of the disturbance, the turning latitudes for many equatorial modes are north of the heating (see appendix B). Thus, as discussed above, modes with positive equivalent

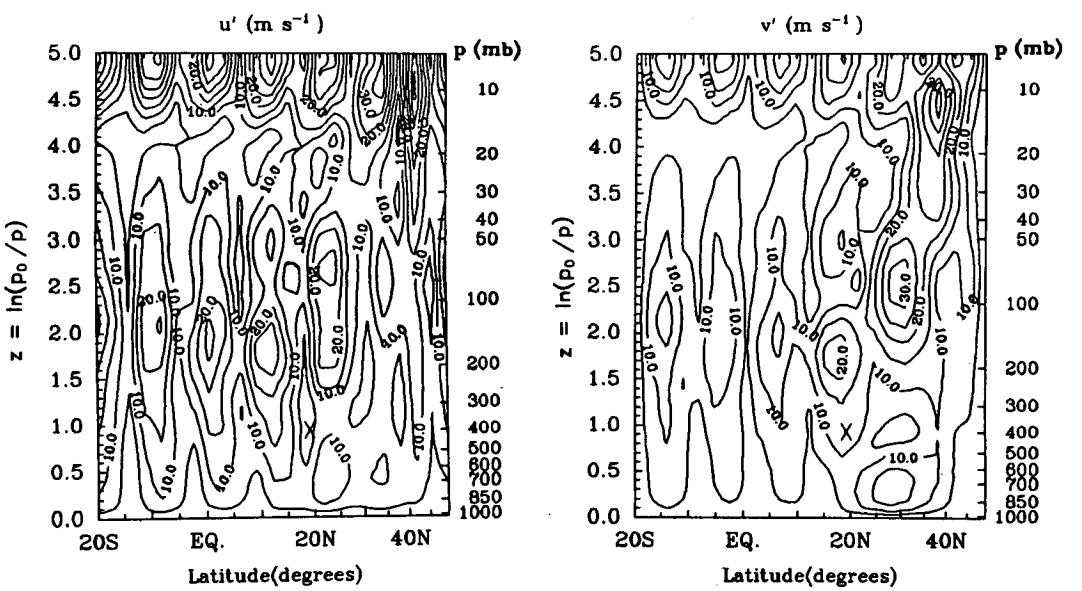

FIG. 3. Meridional and vertical distribution of the amplitudes of u' and v' in experiment B.

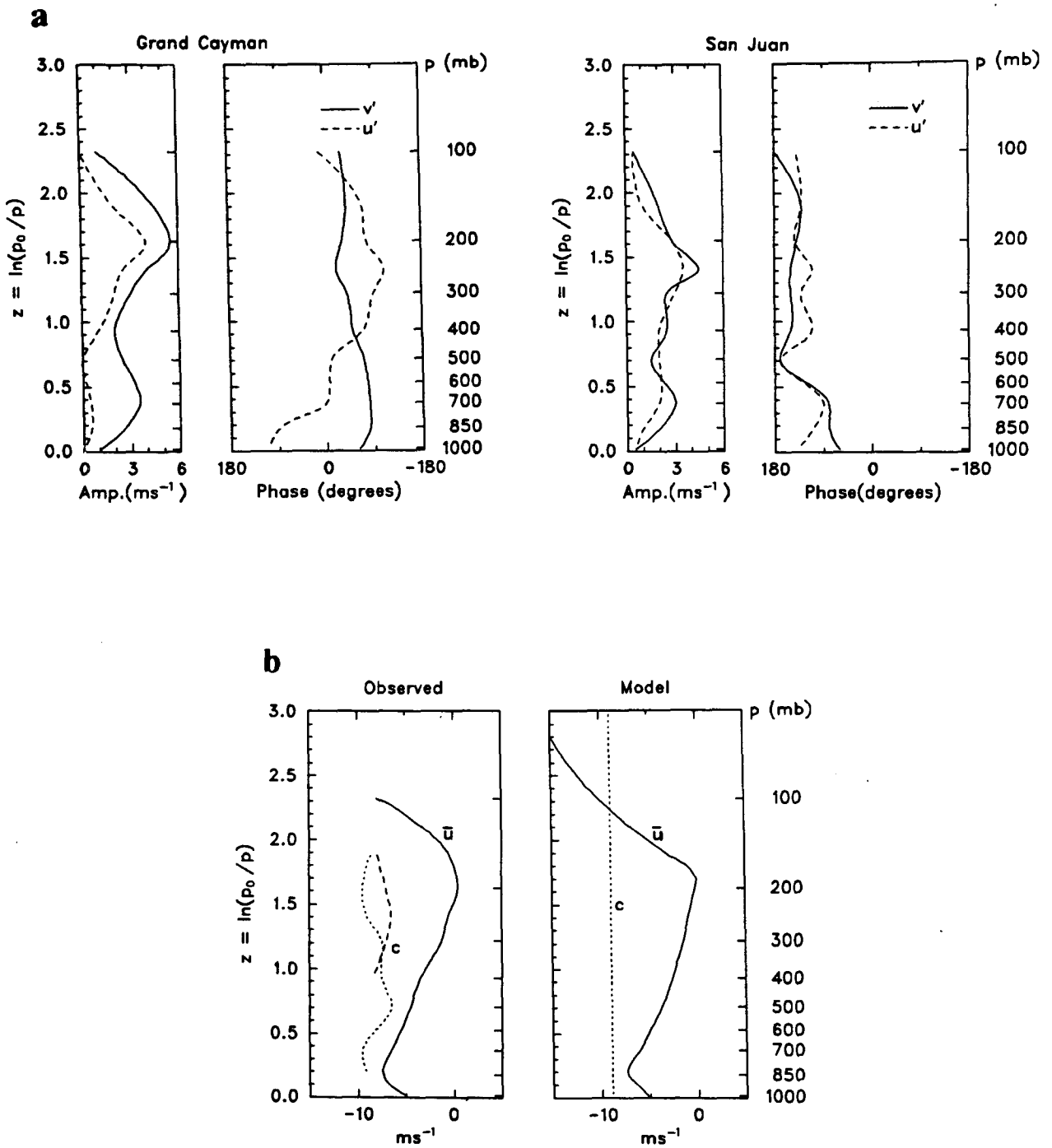

FIG. 4. (a) Amplitudes and phases of u' and v' at Grand Cayman (left) and San Juan (right), from Shapiro (1986). The sign of the phase has been changed to conform to the convention in the present paper. (b) Observed (left-hand panel) $\bar{u}_0(z)$ from Grand Cayman–San Juan average, and phase speed $c(z)$ determined by phase difference in zonal (dashed line) and meridional (dotted line) wind components. Model (right-hand panel) $\bar{u}_0(z)$ and wave phase speed, c, at latitude of maximum heating, used in experiment C.

depths are excited. These are vertically propagating equatorial Rossby waves, with substantial vertical energy flux $[\overline{\mathrm{Re}(w')\,\mathrm{Re}(\Phi')}]$. The domain has been extended both in height and latitude to ensure that the response near the heating is not contaminated by reflection off the boundaries. Near the maximum heating, the maximum amplitude of each wind component is $\sim$25 m s^{-1}, much larger than that in experiment A. The large response is consistent with the results of SLS. Specifically, following the vorticity argument in section

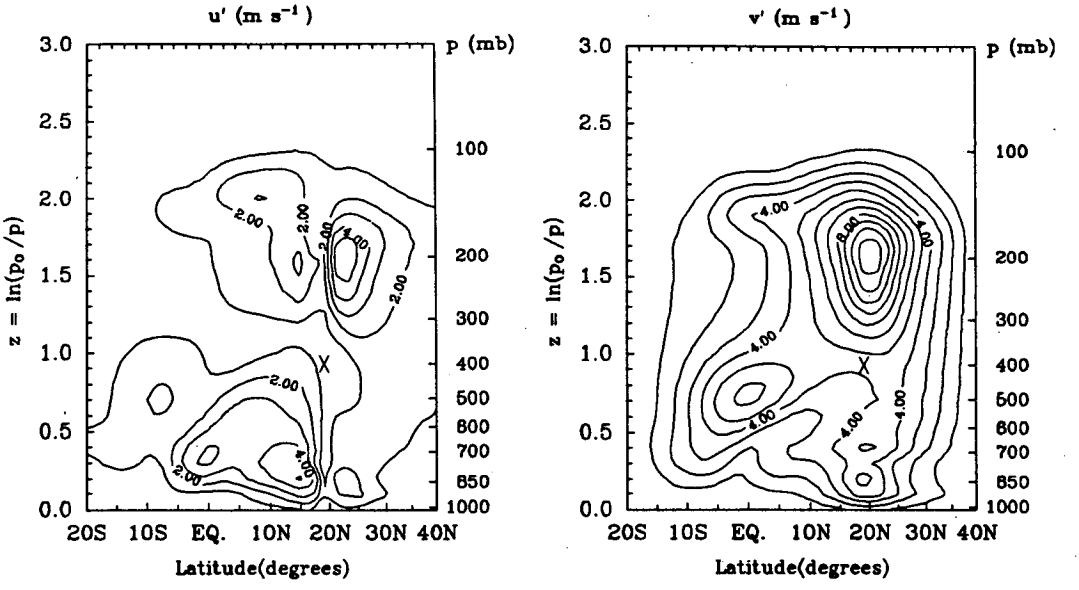

FIG. 5. (a) As in Fig. 2a, but for experiment C. (b) As in Fig. 2b, but for experiment C. The amplitude and phase of u', v', ζ', δ' and Φ' are shown at the latitude of maximum heating (19.0°N), and at one grid point to the north and south.

5 of SLS [and, as a first approximation, neglecting the planetary term 3 in (3)], the amplitude of $\zeta'/\delta' \propto |\hat{\sigma}|^{-1}$ and, therefore, tends to be large for long intrinsic periods. Since δ' is relatively invariant, the amplitude of the response is also $\widetilde{\propto} |\hat{\sigma}|^{-1}$. For the specified intrinsic period of 21 days, the corresponding time scale $|\hat{\sigma}|^{-1}$ = (21 days)/2π = 3.3 days. As a result, both vorticity and wind amplitudes are relatively large.

Of the four basic experiments presented in this paper, only experiment B is significantly affected when cumulus momentum transports are included. The key time scale for these transports is the fastest damping time due to convective detrainment, $|(g/p)\partial \bar{M}_c/\partial z|^{-1}$ ~ 1.4 days at 200 mb and much longer at lower levels (see appendix C). Since the damping time due to convective detrainment is about half the intrinsic time scale of the wave (3.3 days) in experiment B, cumulus transports are effective in reducing the wind amplitudes by about a factor of 2, to ~15 m s^{-1}. For long-period Rossby waves, dissipation corresponding to observed cloud mass fluxes is important.

In other experiments, the largest divergence, near 200 mb, was at a level where the intrinsic time scale $|\hat{\sigma}|^{-1} \sim |\sigma|^{-1} < 1$ day. Since this time scale is much shorter than the detrainment time scale, cumulus transports are ineffective in altering the wave dynamics for experiments A, C and D. Details and implications are discussed in appendix C.

4. Caribbean $\bar{u}(z)$

The study of Shapiro (1986) provides an analysis of the vertical structure of a series of strong easterly waves in the Caribbean. The present model can be used to test the hypothesis that the observed vertical structure was a forced linear response to cumulus convection associated with the disturbances. Shapiro extracted the structure of the easterly wave disturbances with empirical orthogonal functions (EOFs) applied to the combined low-level and 200 mb winds in the 3–5 day band. The most striking feature of the dominant EOF mode for July 1975, as well as other months, was the consistent near 90° westward shift of the vorticity and meridional wind at 200 mb relative to the lower level. One objective of the present study is to provide a dynamical explanation for the westward phase shift.

To resolve the vertical structure of the disturbances, the dominant mode for July 1975 was projected onto time series of island rawindsonde station winds. Figure 4a shows the amplitude and phase of the zonal and meridional wind perturbations at Grand Cayman and San Juan. These stations, both near 19°N, were in the region of largest diagnosed wave amplitude. The meridional wind perturbation at both stations had a westward tilt with height in the lower troposphere. Based on the observed wave period of 4.5 days, and the distance between the stations, a zonal wavelength and phase speed could be deduced. As shown in the left-hand panel of Fig. 4b, the observed phase speed did not substantially vary with height, and for the v' component was about −9 m s^{-1} near 200 and 700 mb, where the wave amplitude was largest. The model assumption that there is a single Fourier component with a given period and wavelength is well approximated.

Although the mean wind varied in all three dimensions, the basic state wind used in experiment C is based

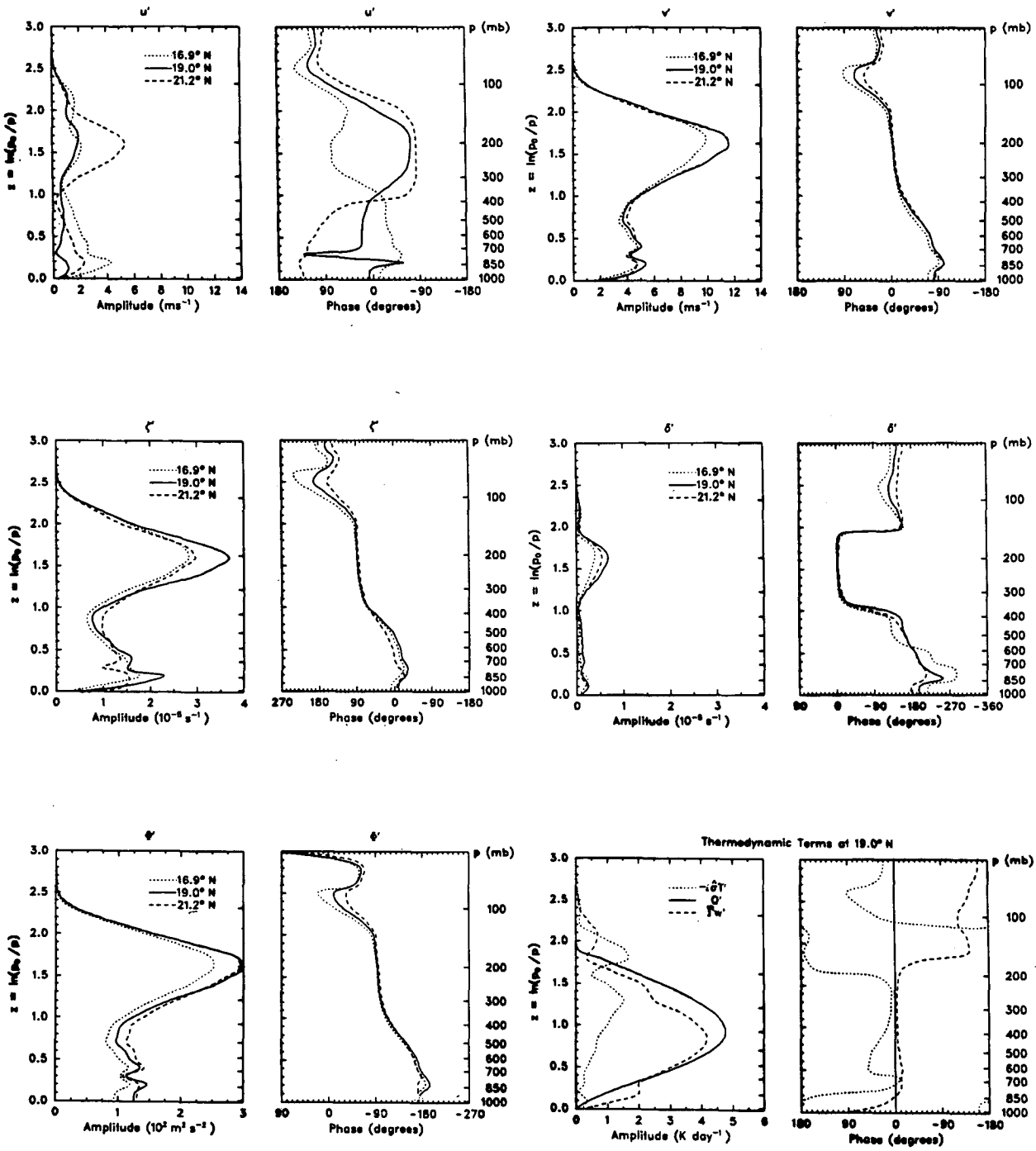

FIG. 5. (*Continued*)

on $\bar{u}_0(z)$ from the Grand Cayman/San Juan mean, shown in the left-hand panel of Fig. 4b. The mean wind has an easterly shear from the surface to 850 mb, where $\bar{u}_0 = -7.5$ m s^{-1}, and a westerly shear from that level up to 200 mb, where $\bar{u}_0 = 0$. To the extent that the vertical structure of the wave is a local linear response to convective forcing, the model results near the latitude of maximum heating should be realistic. The effect of zonal or meridional variations of $\bar{u}$, which are not known for the time of the observations, is beyond the scope of the present paper.

The results of experiment C, using the model wave parameters and the mean zonal wind in the right-hand panel of Fig. 4b (based on the left-hand panel), are

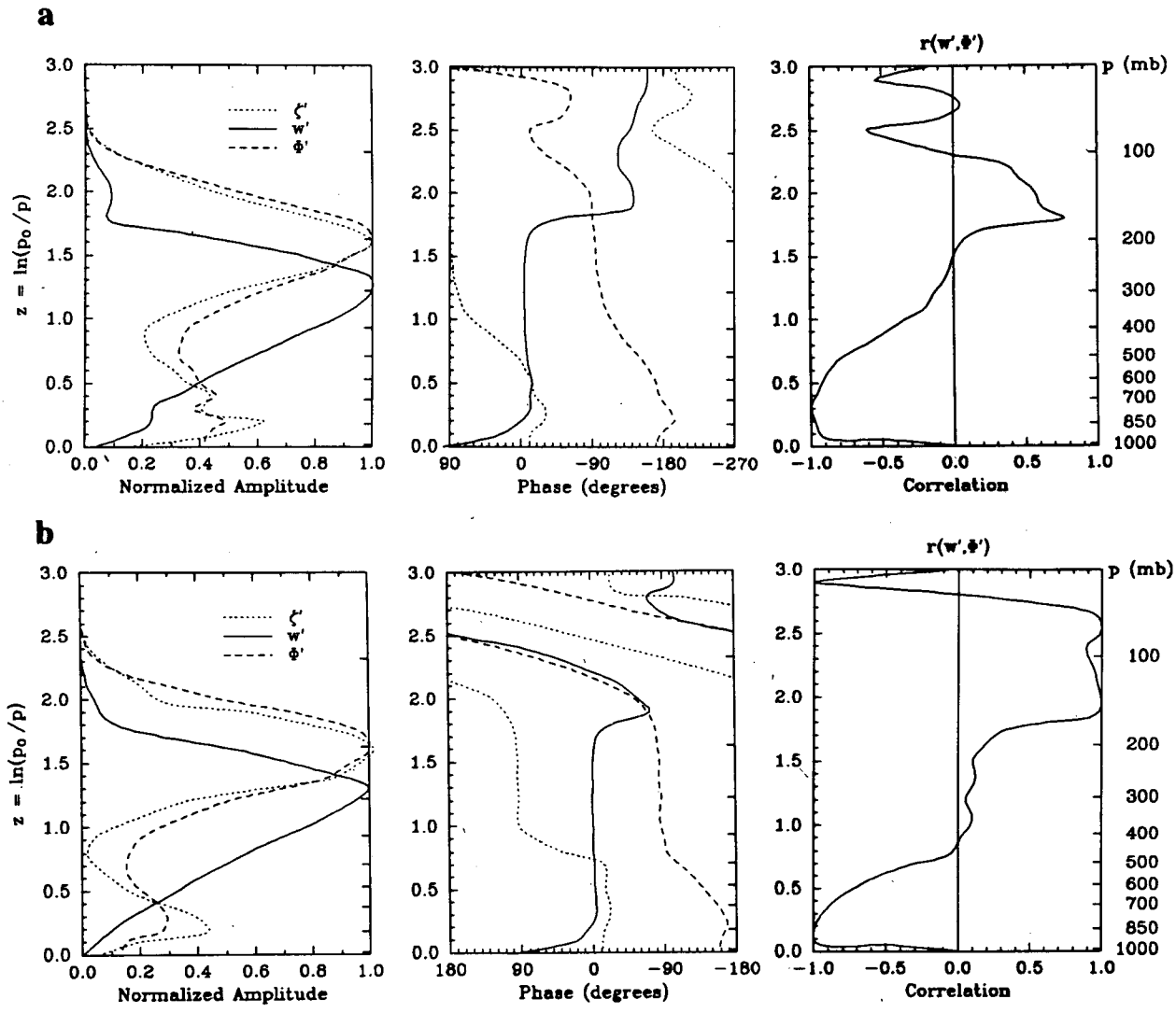

FIG. 6. (a) Amplitude and phase of w', Φ' and ζ' for experiment C at 19.0°N, the latitude of maximum heating. The amplitudes have each been normalized to have maximum value 1.0. Correlation $r(w', \Phi')$ is explained in text. (b) As in (a) but at 8.6°N, for heating centered at that latitude.

given in Fig. 5. The latitude of the maximum heating is taken to be 19°, near the latitude of the island stations. The zonal wind used in the model is $\bar{u}(z) = \bar{u}_0(z)\cos\theta/\cos(19°)$, so that the intrinsic frequency is independent of latitude. The formulation of the experiment is summarized in Table 1. Note that enhanced boundary layer diffusion (see section 2) is included. The domain of the model has been extended to the south to allow meridional propagation of energy across the equator. For consistency with section 3, the meridional and vertical structure of the heating Q' are taken to be the same as in Fig. 1. Given the lack of knowledge of the true distribution of the heating, as well as the three-dimensional structure of $\bar{u}$, the present experiment can only give a general indication of the wave's complete structure.

Figure 5 shows a small eastward tilt of v' and ζ' with height from the surface to about 850 mb, and a strong westward tilt above that level. There is little variation in the phase of v' or ζ' with latitude near the maximum heating. The phase of v' and ζ' near 200 mb are nearly 90° to the west of the corresponding phase near the surface. These results are all in agreement with the observations in Shapiro (1986), including those shown in Fig. 4a. The structure of v' agrees with the other studies noted in the Introduction, particularly the composite results of Burpee (1980). *It is especially noteworthy that the trough tilts in the direction opposite to the wind shear (i.e., westward tilt with westerly mean shear), unlike the tilt/shear relationship of Holton's cases II and III.*

The phase of u' is more variable in both the obser-

vations and model results, and is less easily defined. The maximum amplitude of u' in experiment C, which is slightly to the north of the heating maximum, is ~ 6 m s^{-1}, or about a factor of 1.5 larger than that in Fig. 4a. The amplitude of v' in experiment C is ~ 12 m s^{-1}, or about a factor of 2.5 larger than that in Fig. 4a. Thus, a reduction of the heating rate by a factor of 2 will nearly reconcile the observations with the model results. The response depends on the vertical and meridional distribution, as well as the magnitude, of the heating. Although the magnitude and vertical distribution are typical for tropical systems, the extent to which the actual heating that forced the observed waves had the same magnitude and distribution is unknown.

The westward shift of the trough axis from the near-surface to 200 mb level can be explained in terms of vertical energy flux in a vertically varying basic state zonal wind. The response combines features of experiments A and B. As in experiment A, the warming rate following the mean wind ($-i\hat{\sigma}T'$) is small in comparison with adiabatic cooling ($\bar{\Gamma}w'$); therefore w' tends to follow Q', with divergence above and convergence below the heating maximum. In the upper troposphere, above the heating maximum, $-\hat{\sigma} \sim -\sigma$ so that, as in experiment A, vertically trapped modes[2] are primarily forced; w' tends to be in quadrature with Φ', so that the correlation between w' and Φ' is small. Figure 6a shows the amplitude and phase of w', Φ' and ζ' at the latitude of maximum heating for experiment C (19°N), together with the correlation between w' and Φ':

$$r(w', \Phi') \equiv \mathrm{Re}(w'\Phi'^*)/(|w'\Phi'^*|)$$
$$= \cos[\mathrm{phase}(w') - \mathrm{phase}(\Phi')].$$

Note that $\mathrm{Re}(w'\Phi'^*)$, representing the real part of the product between w' and the complex conjugate of Φ', is twice the vertical energy flux, $\overline{\mathrm{Re}(w')\,\mathrm{Re}(\Phi')}$. When the correlation is small, w' and Φ' are nearly in quadrature and there is relatively little vertical energy flux. When the correlation is large, w' and Φ' are nearly in phase or 180° out of phase, so that most of the energy flux is either upward ($r > 0$) or downward ($r < 0$).

In the upper troposphere, the twisting term in the inviscid vorticity budget (3) is much smaller than the stretching term, v' is in quadrature with ζ', and the magnitude of the planetary term ($\beta v'$) is less than that of the tendency term ($-i\hat{\sigma}\zeta'$). Thus, as in experiment A, the vorticity in experiment C in the upper troposphere above the heating maximum is 90° to the west of the heating Q', and Φ' is about 90° to the east.

In the region $2.3 > z > 1.5$, above the heating maximum, the vertical energy flux is upward. A critical level at $z \approx 2.2$, where $\bar{u} = c$, absorbs the upward flux. Above $z = 2.3$ the amplitudes of w' and Φ', and thus the energy flux, are very small.

Below the heating maximum the energy flux is downward, toward the ground. The magnitude of the wave's intrinsic frequency decreases downward, as the near-critical level is approached at $z = 0.2$, where $\bar{u} \approx c$. As evident in the stronger correlation between Φ' and w', the wave is in a region that supports a vertical energy flux, as in experiment B. The near-critical level near the ground provides a region where dissipative effects become important. At $z = 0.1$, the diffusion term 6 in the vorticity budget (2) is nearly equal in magnitude to the stretching term 4; above that level it is less than 25%. Since the phase of w' is locked to approximately 0° by the heating, downward flux requires Φ' to have a phase $< -90°$. Thus, there is a westward phase shift in Φ' with height between the near-surface and 200 mb levels. Close to the ground, Φ' and w' are nearly 180° out of phase, so that almost all of the energy flux is downward. The results suggest that the downward incident energy is absorbed, with little reflection off the ground. The vorticity is close to geostrophic balance with the height field, $f\zeta' \sim \nabla^2\Phi'$, and is of opposite sign. The westward shift of the vorticity

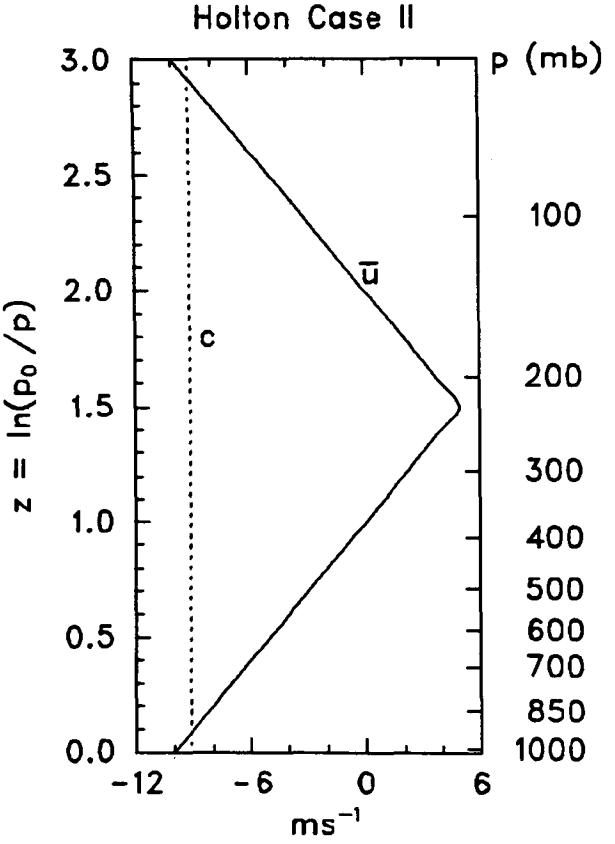

FIG. 7. The value of $\bar{u}_0(z)$, after Holton (1971), case II, used in experiment D. The wave phase speed c at the latitude of maximum heating is also shown.

[2] Strictly speaking, horizontal modes are ill defined in a vertically sheared zonal flow. For weak shear, however, a modal decomposition is still useful in a WKB sense, following Lindzen (1971, 1972).

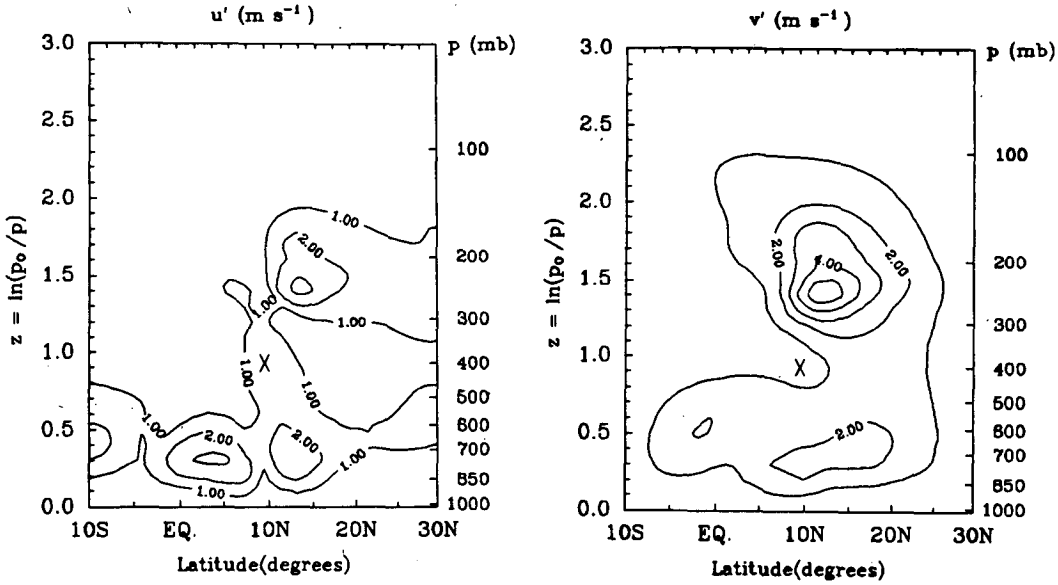

FIG. 8. (a) As in Fig. 5a, but for experiment D. (b) As in Fig. 5b, but for experiment D, with heating centered at 9.4°N.

trough in experiment C is thus the natural consequence of the downward energy flux below the maximum heating, into a region of strong absorption.

Conversely, the absence of a near-critical level, as in the extreme case of experiment A, led to a near-quadrature of w' and Φ' below the heating maximum. The absence of a downward energy flux in that counterexample confirms the importance of the absorption of energy in the vicinity of the near-critical level near the ground for the wave's vertical structure.

Given the uncertainties in the specification of the heating, as well as the explicit omission of the zonal and meridional structure of the mean zonal wind, the rough agreement between the (adjusted) model amplitudes and the observations is encouraging. Moreover, the vertical phase structure of the response of the present model is clearly closer to the observations than are either Holton's case II results or the classical easterly wave model itself. *The results emphatically support the hypothesis that the waves analyzed by Shapiro (1986) were convectively forced disturbances with vertical structure determined by linear dynamics.*

The vertical structure of the response depends on the latitude of the specified heating. Figure 6b shows the response when the maximum heating is at 9°N. At this lower latitude, the minimum vorticity near 500 mb is smaller, and the transition across the level of maximum heating is sharper. The near 90° westward phase shift of vorticity, in particular, occurs over a more narrow layer, with nearly constant phase below about 500 mb.

5. Holton's case II

We now investigate the contrasting relationship between the wave tilt and mean wind shear found in section 4 and that found in Holton's (1971) experiments. In order to evaluate the sensitivity of the forced response to the vertical profile of the mean zonal wind $\bar{u}$, Holton considered several nonresting basic states. His case II, which included a westerly shear from the surface to 12 km, was considered typical of the easterly trade wind regime. Holton assumed $\bar{u} = \bar{u}_0(z)\cos\theta$, so that $\hat{\sigma}$ was independent of latitude. The vertical profile of $\bar{u}_0(z)$, based on Holton's case II, is given in Fig. 7. This mean wind is similar to that used in experiment C (Fig. 4b), but has a true critical level at the ground, and a westerly wind of 5 m s^{-1} near 200 mb. In Fig. 8, the results of experiment D are shown, using this mean zonal wind in the present model. The center of the heating is at 9.4°N. Figure 8 is very similar to Holton's case II results. The maximum amplitude of the meridional wind in experiment D is ~6 m s^{-1}, nearly the same value as in Holton's case II solutions.

As in Holton's solution, the surface trough (as defined by the phase of vorticity) in experiment D near the latitude of maximum heating is to the west of the heating maximum, and there is a general eastward tilt of v' with height below the level of maximum heating. These features are similar to the classical easterly wave model. In the present case, however, there is a variation of the phase of v' with latitude not evident in Holton's solution. At latitude 7.4°N, to the south of the maximum heating, the eastward tilt of v' above about 600 mb is greater; at latitude 11.4°N, to the north, the tilt is more to the west. The inclusion of scale-independent dissipation with a damping time of 2.65 days in the present model (results not shown) substantially reduced the variation in the phase of v' with latitude near the maximum heating, agreeing much more closely with Holton's case II solution. The meridional variation of phase, with or without damping included, is seen even

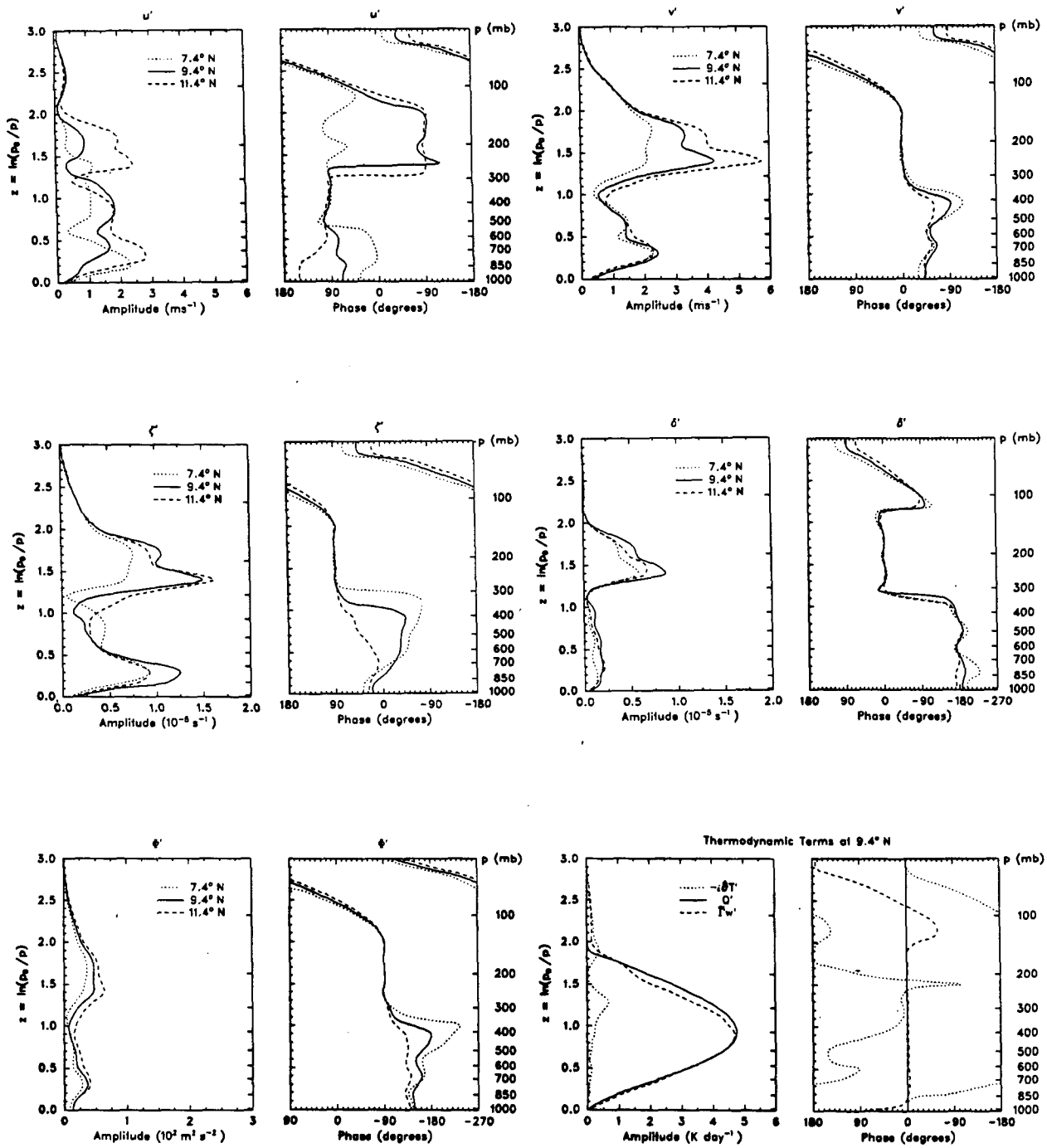

FIG. 8. (*Continued*)

more clearly in ζ' than v' (Fig. 8). To the north of the maximum heating, ζ' tilts westward above about 700 mb.

The dependence of the vertical phase structure on the latitude of convective heating is made explicit in Fig. 9. The figure has the same format as Fig. 6, with Fig. 9a for the response to a heat source centered at 9°N (experiment D), and Fig. 9b for the source centered near 19°N. The phase structure of the response at 19°N in Fig. 9b is very similar to that of experiment C (Fig. 5 and Fig. 6a), which has the source centered at the same latitude. *The zonal wind profile specified in Holton's case II leads to a westward tilt with height above 700 mb when the heat source is centered at this higher latitude.* There is downward energy flux below 200 mb, toward the critical level at the surface. By contrast, the response to a source at 9°N (experiment D; Fig. 8 and Fig. 9a) has an eastward tilt below 400 mb, with a rapid

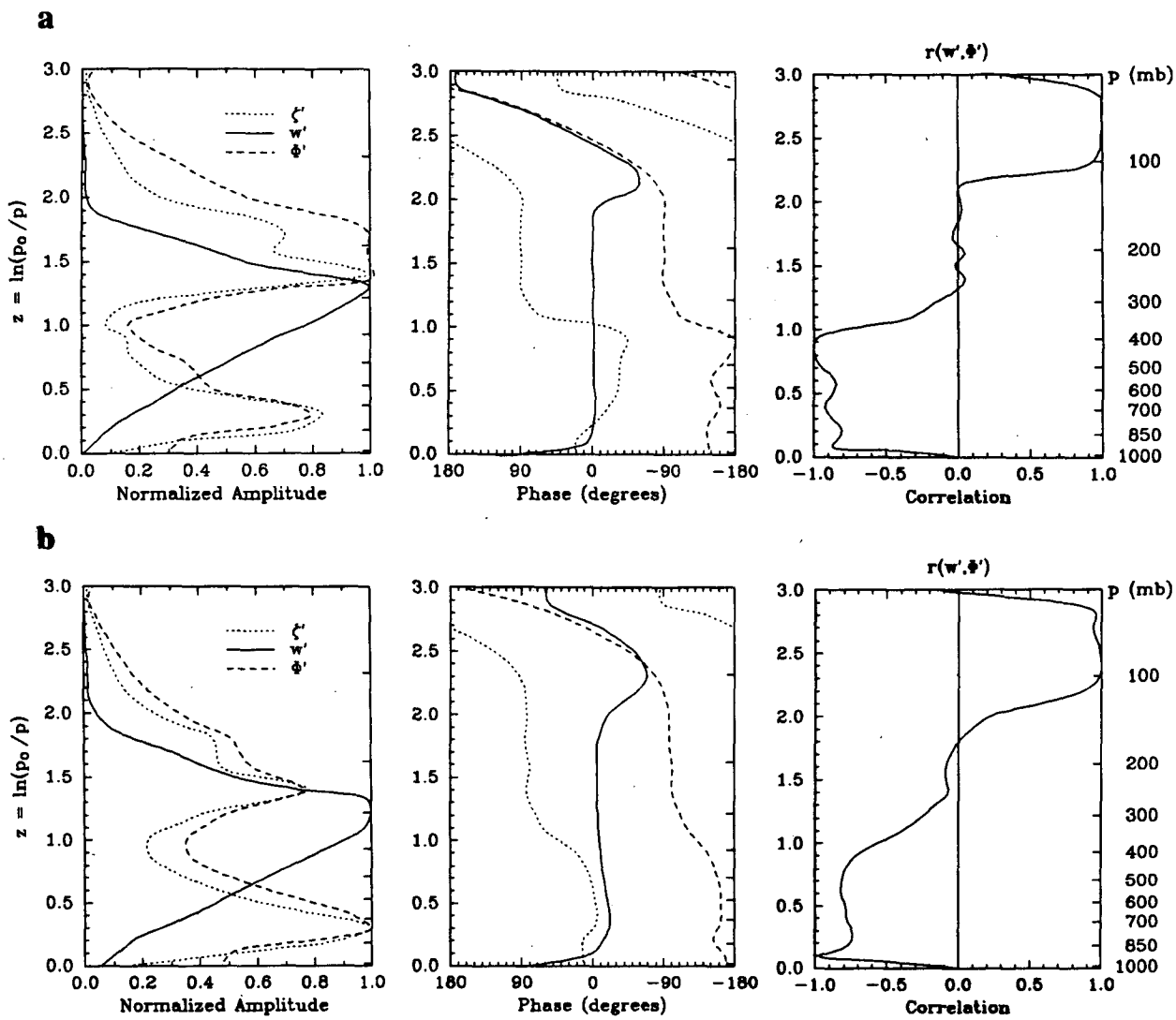

FIG. 9. (a) As in Fig. 6a, but for experiment D at 9.4°N, the latitude of maximum heating. (b) As in (a) but at 19.4°N, for heating centered at that latitude.

westward phase shift across the level of maximum heating. As in Fig. 6b, for the Caribbean zonal wind profile, the lower latitude has produced a more narrow layer of transition. The net westward phase shift of the trough axis between 850 and 200 mb for heating at either latitude emphasizes once again the importance of the downward energy flux for the wave's vertical structure.

6. Conclusion

Very good agreement was found between the vertical structure of the waves observed by Shapiro (1986) and the model-derived structure in section 4 (experiment C). The 90° westward phase shift between the 200 mb and near-surface troughs, and the westward tilt of the trough axis with height, appear to be a direct consequence of the interaction between the forced wave and its environment. The zonal wind was assumed to be a function of height, taken from observations near the latitude of largest wave amplitude. It is possible that the use of a more realistic zonal wind distribution could change the structure of the wave response; however, the success of the simulation suggests that we have captured the essence of the Caribbean wave dynamics. After adjustment of the magnitude of the heating, the amplitudes of the zonal and meridional winds predicted in experiment C were found to be close to those observed. Although linearization is not strictly valid for the wind amplitudes ~ 5 m s^{-1}, the model's linear dynamical framework appears to well represent the wave's structure; consideration of why nonlinear terms can be neglected and yet a realistic structure obtained is left for further study. The westward shift of the trough

axis in the model solutions was found to depend on the downward flux of wave energy toward a near-critical level near the ground, where the intrinsic period was long. The results suggested that the downward incident energy was absorbed, with little reflection off the ground.

It is also clear that the eastward tilt of the trough axis in the classical picture of the Caribbean easterly wave is not a simple consequence of the vertical profile of the mean zonal wind. Experiments described in sections 4 and 5 imply that the latitude of the disturbance may be as important a factor in the determination of the direction of the tilt as is the structure of the mean zonal wind. Using Holton's (1971) case II basic state zonal wind, with westerly shear in the lower and middle troposphere, a westward tilt above 700 mb was found at the latitude of maximum heating when centered at 19°N; an eastward tilt was favored below 400 mb when the heating was more to the south, near 9°N (section 5, experiment D). In the latter case, the westward phase shift occurred over a narrow layer near the level of maximum heating. The reason for this variation with latitude remains to be understood.

Finally, we note that the amplitude of the response depends not only on the magnitude of the heating, but also on its meridional scale. For consistency with Holton (1971), the decay scale for the Gaussian profile of heating was taken to be 3° latitude. Other experiments (results not shown) that used a heating with larger meridional extent produced larger wind amplitudes. The maximum amplitudes of the winds were roughly proportional to the meridional scale. Inspection of the results indicated that the magnitude of the divergence and vorticity were almost independent of the meridional scale of the heating. Apparently the winds were stronger simply because, for the same horizontal gradient (vorticity and divergence), their meridional scale of variation was larger. The true meridional scale of the heating that forced the disturbances analyzed by Shapiro (1986) is not known. The magnitude of the heating that is projected from the mesoscale-organized convection onto the synoptic-scale wave is another question that is not easily addressed.

Acknowledgments. The authors wish to thank Drs. K. V. Ooyama and H. Willoughby for their very helpful comments on an earlier version of this paper. Partial support for the CSU authors was provided by National Science Foundation Grants ATM-8305759 and ATM-8609731 to the Department of Atmospheric Science, Colorado State University.

APPENDIX A

List of Symbols

$\mathbf{F}_c$	cumulus momentum source
H	scale height
M_c	cumulus mass flux
Q	diabatic heating rate
T	temperature
a	radius of earth (6.37×10^6 m)
c	σ/k, wave phase speed
c_p	specific heat at constant pressure ($1004\ m^2\ s^{-2}\ K^{-1}$)
f	$2\Omega \sin\theta$, Coriolis parameter
g	gravitational acceleration
h	equivalent depth
k	$s/(a\cos\theta)$, inverse of wave's zonal scale
$\mathbf{k}$	vertical unit vector
p	$p_0 \exp(-z)$
p_0	surface pressure (1015 mb)
$r(w', \Phi')$	correlation between w' and Φ', defined in section 4
R	gas constant ($287\ m^2\ s^{-2}\ K^{-1}$)
s	longitudinal wavenumber
t	time
T	temperature
$\mathbf{u} = (u, v)$	(zonal, meridional) velocity
$\mathbf{u}_c$	velocity at cloud base z_c
w	dz/dt, vertical velocity
z	$\ln(p_0/p)$, vertical coordinate
z_c	cloud base ($z = 0.1$, $p = 918$ mb)
α	damping rate for Rayleigh friction and Newtonian cooling
β	$(df/d\theta)/a$
δ	divergence
λ	longitude, positive to the east
Ω	angular speed of earth's rotation
Φ	geopotential
ν	kinematic coefficient of viscosity and thermal diffusion
σ	angular frequency of wave perturbation
$\hat{\sigma}$	$\sigma - k\bar{u}$, Doppler-shifted (intrinsic) frequency; intrinsic period $= 2\pi/\lvert\hat{\sigma}\rvert$
θ	latitude
ζ	vorticity
$\bar{\Gamma}$	thermodynamic stability, $\partial\bar{T}/\partial z + \kappa\bar{T}$, where $\kappa = R/c_p$.
$\overline{\mathrm{Re}(w')\,\mathrm{Re}(\Phi')}$	Vertical energy flux. Re( ) represents the real part of the complex variable; the overbar represents the average over a wave cycle.

APPENDIX B

Solution of the Vertical Structure Equation for Vertical Velocity

Consider the nth forced mode in a separable problem, with frequency σ and constant static stability $\bar{\Gamma}$. The vertical structure of this mode is governed by the separation relation [e.g., Eq. (2.81) of Holton, 1975],

$$dw_n/dz - w_n = [-i\sigma/(gh_n)]\Phi_n \quad \text{(B1)}$$

and the hydrostatic thermodynamic energy equation

$$[-i\sigma/R]d\Phi_n/dz + \bar{\Gamma}w_n = Q_n, \quad \text{(B2)}$$

where primes denoting perturbation quantities have been dropped for convenience. Here h_n is the nth equivalent depth, determined by the horizontal eigenvalue problem as in Lindzen (1967) and $Q_n(z)$ is the vertical structure of the projection of the heating onto the nth mode, and similarly for $w_n(z)$ and $\Phi_n(z)$. The vertical structure equation for w_n can be obtained by eliminating Φ_n between (B1) and (B2):

$$[d^2/dz^2 + \Lambda_n][w_n \exp(-z/2)]$$

$$\text{[I]} \quad \text{[II]}$$

$$= [R/(gh_n)] \exp(-z/2)Q_n(z), \quad \text{(B3a)}$$

where

$$\Lambda_n = (R\bar{\Gamma})/(gh_n) - 1/4. \quad \text{(B3b)}$$

The solution for w_n is well approximated by the local balance between the heating and term II in (B3a),

$$\Lambda_n w_n(z) = R/(gh_n)Q_n(z) \quad \text{(B4)}$$

as long as term I is much less than term II. For simplicity, suppose that the tropospheric heating has the form

$$Q_n(z) = \begin{cases} \sin(\mu z) \exp(z/2), & 0 \leqslant z \leqslant \pi/\mu \\ 0, & z \geqslant \pi/\mu. \end{cases} \quad \text{(B5)}$$

This form approximates profiles of heating typically observed, where (as in the heating specified in Fig. 1) $\mu \approx \pi/2$. Then, term I in (B3a) is much less than term II when

$$\Lambda_n \gg \mu^2 \approx 2.5. \quad \text{(B6)}$$

To understand the circumstances under which this condition is valid, one can use the midlatitude equivalent to (1b),

$$L(\theta) = -\beta k/\sigma - k^2 + \sigma^2/(gh) - f^2/(gh), \quad \text{(B7)}$$

which is a valid approximation for the vertically trapped modes in experiment A. The heating in Fig. 1, with meridional scale ~300 km, will tend to project onto horizontal modes with $L \sim (300 \text{ km})^{-2}$. Using the values for σ and k of experiment A, and a typical tropospheric value of $R\bar{\Gamma}/g \approx 600$ m, (B7) can then be solved for h and thus Λ. At latitude $\theta = 9°$N, $h \approx -3$ m and $\Lambda \approx -200$; at $\theta = 19°$N, $h \approx -20$ m and $\Lambda \approx -30$. Thus, condition (B6) is satisfied when the heating is centered at 9°N, or even twice as far from the equator. Since $R\bar{\Gamma}/g \gg h$, (B4) together with (B3b) imply

$$\bar{\Gamma}w \approx Q \quad \text{(B8)}$$

so that the warming rate,

$$[-i\sigma/R]d\Phi/dz = Q - \bar{\Gamma}w, \quad \text{(B9)}$$

is small. In the model solution for experiment A, with the source at 9°N, the measure of the degree of local balance $|(Q - \bar{\Gamma}w)/\bar{\Gamma}w|$ is found to be ~0.1 (cf. thermodynamic terms in Fig. 2b); the same measure is ~0.3 when the source is at 19°N.

The present analysis can be extended to nonzero mean zonal wind with intrinsic (Doppler-shifted) frequency $\hat{\sigma} \neq \sigma$. If the vertical shear of the zonal wind is not too large, a modal analysis for constant intrinsic frequency will be locally valid. (See footnote 2 in section 4.) For small intrinsic frequency [$|\hat{\sigma}| \ll 2\pi/(5 \text{ days})$], solution of the dispersion relation for equatorial modes (Eq. (36) of Lindzen, 1967) indicates that the turning latitudes for many modes are poleward of the tropical heat sources specified here. Thus, modes with positive equivalent depth will be excited. As long as the narrow heat source is primarily projected onto modes with $|h| \ll 240$ m, the condition (B6) and the local balance (B8) will still be valid. In practice, for experiment B with $\hat{\sigma} = -2\pi/(21 \text{ days})$ and latitude 19°N, the measure of the degree of local balance $|(Q - \bar{\Gamma}w)/\bar{\Gamma}w| \sim 0.4$.

APPENDIX C

Cumulus Momentum Transports: Implementation and Results

When included, the cumulus momentum source term for the perturbation is parameterized as

$$\mathbf{F}'_c = (g/p)(\partial/\partial z)[\bar{M}_c(\mathbf{u}' - \mathbf{u}'_c) + M'_c(\bar{\mathbf{u}} - \bar{\mathbf{u}}_c)], \quad \text{(C1)}$$

as in Eqs. (1) and (2) of Rosenlof et al. (1986). Here $\bar{M}_c$ is the cumulus mass flux associated with the basic state, and M'_c with the perturbation; $\bar{\mathbf{u}}_c$ and $\mathbf{u}'_c$ are the corresponding velocities at cloud base ($z = 0.1$, $p = 918$ mb). The cumulus mass flux profile M_c, used for both the mean and perturbation, is given in Fig. C1. The cloud base mass flux is 5 mb h^{-1}, consistent with the precipitation rate of 1 cm day^{-1}. The damping time due to detrainment by the basic state mass flux is $|(g/p)\partial\bar{M}_c/\partial z|^{-1}$, which is ~1.4 days at 200 mb.

When cumulus momentum transports were incorporated in experiment A, with period 5 days and intrinsic time scale 5 days/$2\pi \sim 0.8$ day, the maximum of v' near 200 mb decreased by much less than 1 m s^{-1}. Since the intrinsic time scale is shorter than the detrainment time scale (~1.4 days), cumulus momentum effects cannot substantially affect the amplitude of the response.

For experiment B, the longer intrinsic time scale of 3.3 days exceeded the detrainment time scale, so that cumulus momentum transports could dampen the wave amplitude by playing a significant role in the local vorticity budget.

For experiment C, with a realistic Caribbean mean zonal wind, the 200 mb detrainment region had a mean wind approximately zero and therefore an intrinsic time scale 4.5 days/$2\pi \sim 0.7$ day, half the detrainment

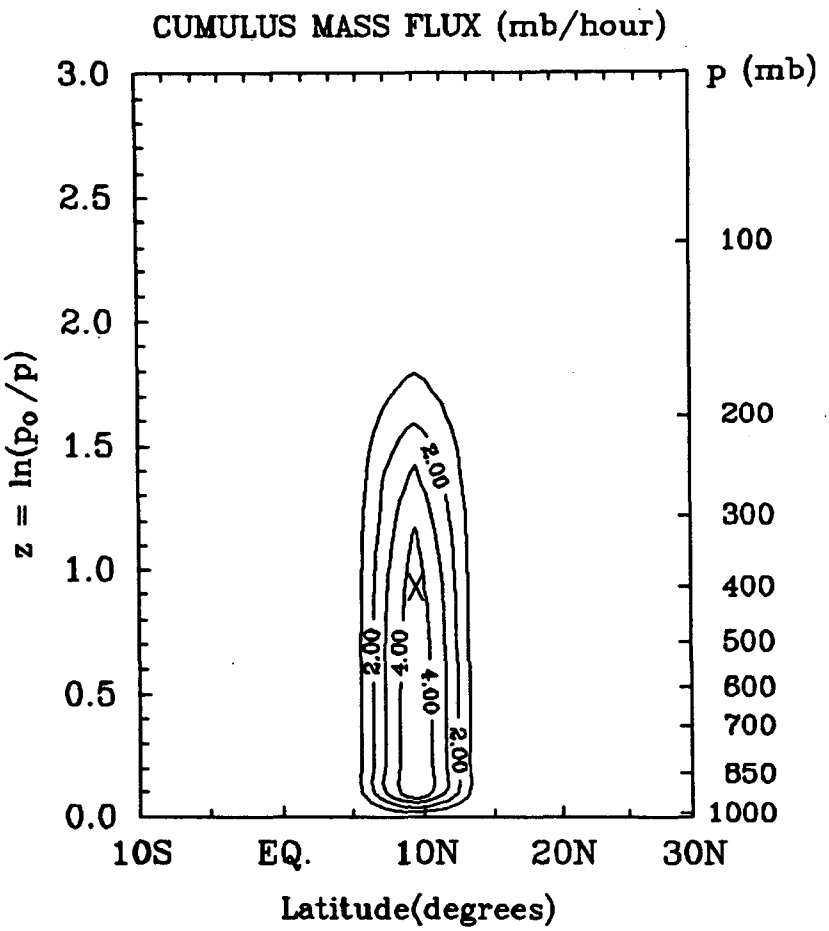

FIG. C1. Cumulus mass flux used as $\bar{M}_c$ and M'_c.

time scale. Consequently, cumulus momentum transports did not substantially change the structure or the maximum response amplitude. The results of experiment D [Holton's (1971) case II] were similar.

The waves of experiments A, C and D have relatively short intrinsic periods (~5 days) at the level of maximum perturbation divergence, 200 mb. Clearly they cannot be considered internal Rossby waves with long intrinsic period. Without cumulus momentum transports, all wind amplitudes were ~ 10 m s^{-1} in the upper troposphere. Inclusion of cumulus momentum transports with a damping time longer than the local (intrinsic) wave time scale does not qualitatively affect the atmosphere's response to the heating. This conclusion extends the argument of Stevens et al. (1977), obtained in a uniform mean zonal flow, to a vertically sheared flow by applying the same logic to the local time scales in the upper troposphere. The perturbation response in the upper troposphere appears to play the dominant role in setting wave amplitudes since 1) divergence tends to be largest in that region; 2) divergence, through the vorticity dynamics, drives the vorticity response in both amplitude and phase; and 3) cumulus momentum transports will first affect wave response locally in the upper troposphere (if at all).

Our experiments A and D mimic the cases I and II considered by Holton (1971). The wind amplitudes ~ 10 m s^{-1} resulted from local forced gravity wave dynamics in the upper troposphere, and not from excessive damping of internal Rossby waves as suggested by Stevens et al. (1977). Internal Rossby wave dynamics are in fact irrelevant for these cases because the intrinsic period was not sufficiently long at the level of maximum divergence. Cumulus friction is not required to bring wave amplitudes into the observed range.

REFERENCES

Burpee, R., 1980: The structure of easterly waves during GATE. *Proc. Seminar on the Impact of GATE on Large-scale Numerical Modeling of the Atmosphere and Ocean.* Woods Hole, Mass., National Research Council. [Available from the U.S. Committee for the Global Atmospheric Research Program, 2101 Constitution Avenue, Washington, DC 20418.]

Colón, J., and W. Nightingale, 1963: Development of tropical cyclones in relation to circulation patterns at the 200-mb level. *Mon. Wea. Rev.*, **91**, 199–207.

Fett, R., 1966: Upper-level structure of the formative tropical cyclone. *Mon. Wea. Rev.*, **94,** 9–18.

Holton, J., 1971: A diagnostic model for equatorial wave disturbances: The role of vertical shear of the mean zonal wind. *J. Atmos. Sci.*, **28,** 55–64.

——, 1975: *The Dynamic Meteorology of the Stratosphere and Mesosphere. Meteor. Monogr.*, **15,** Amer. Meteor. Soc.

Johnson, R., 1984: Partitioning tropical heat and moisture budgets into cumulus and mesoscale components: Implications for cumulus parameterization. *Mon. Wea. Rev.*, **112,** 1590–1601.

Jordan, C., 1958: Mean soundings for the West Indies area. *J. Meteor.*, **15,** 91–97.

Lindzen, R., 1967: Planetary waves on beta-planes. *Mon. Wea. Rev.*, **96,** 441–451.

——, 1971: Equatorial planetary waves in shear: Part I. *J. Atmos. Sci.*, **28,** 609–622.

——, 1972: Equatorial planetary waves in shear: Part II. *J. Atmos. Sci.*, **29,** 1452–1463.

Riehl, H., 1954: *Tropical Meteorology.* McGraw-Hill, 392 pp.

Rosenlof, K., D. Stevens, J. Anderson and P. Ciesielski, 1986: The Walker circulation with observed zonal winds, a mean Hadley circulation and cumulus friction. *J. Atmos. Sci.*, **43,** 449–467.

Shapiro, L., 1986: The three-dimensional structure of synoptic-scale disturbances over the tropical Atlantic. *Mon. Wea. Rev.*, **114,** 1876–1891.

Stevens, D., and P. Ciesielski, 1984: A global model of linearized atmospheric perturbations: Model description. Atmos. Sci. Paper No. 377, Colorado State University, Dept. of Atmos. Sci., Fort Collins, CO, 80523, 86 pp.

——, R. Lindzen, and L. Shapiro, 1977: A new model of tropical waves incorporating momentum mixing by cumulus convection. *Dyn. Atmos. Oceans,* **1,** 365–425.

Yanai, M., 1968: Evolution of a tropical disturbance in the Caribbean Sea region. *J. Meteor. Soc. Japan,* **46,** 86–109.